Spin-lattice coupling mediated giant magnetodielectricity across the spin reorientation in Ca₂FeCoO₅

Gaurav Sharma,[1] Shekhar Tyagi,[1] V. R. Reddy,[1] A. M. Awasthi,[1] R. J. Choudhary,[1] A. K. Sinha,[2] and Vasant Sathe[1,*]

[1]*UGC-DAE Consortium for Scientific Research, D. A. University Campus, Khandwa Road, Indore-452001, India*
[2]*Indus Synchrotrons Utilization Division, Raja Ramanna Centre for Advanced Technology, Indore-452013, India*

The structural, phonon, magnetic, dielectric, and magnetodielectric responses of the pure bulk brownmillerite compound Ca₂FeCoO₅ are reported. This compound showed giant magnetodielectric response (10–24%) induced by strong spin-lattice coupling across its spin reorientation transition (150–250 K). The role of two Debye temperatures pertaining to differently coordinated sites in the dielectric relaxations is established. The positive giant magnetodielectricity is shown to be a direct consequence of the modulations in the lattice degrees of freedom through applied external field across the spin reorientation transition. Our study illustrates control of magnetodielectricity by the spin reorientation transition in a material that possesses strong spin-lattice coupling.

I. INTRODUCTION

Magnetodielectric compounds hold great promise due to potential applications in futuristic devices [1,2]. In such compounds, the mutual effective control of electrical and magnetic properties holds the key for promising applications. The number of materials showing such effects are scarce due to the mutual exclusion of spontaneous electrical dipolar order and spin order for electronic reasons; the essentiality for magnetic ordering is partially filled d bands which hinders the dipolar ordering [3,4]. In order to circumvent this condition, compounds showing spiral spin ordering are thought to be promising candidates as the spiral spin order destroys locally the centrosymmetry of the ions enabling polarization. However, the magnetodielectric or magnetoelectric effect in such compounds is found to be very weak, barring few compounds [5,6]. The incommensurate spiral spin arrangement is suggested to be the root cause for the induced polarization in CuO [7], while, the charge ordering of Fe^{2+} and Fe^{3+} is suggested to be responsible for induced ferroelectricity in $LaFe_2O_4$ [8]. On the other hand, geometric frustration is attributed to the improper ferroelectricity observed in yttrium manganites [9]. In partially ordered double-perovskite La_2NiMnO_6, it is shown that the antisite disorder of the cations generates significant asymmetric hopping under magnetic field, resulting in giant magnetodielectric effect at room temperature [10]. In most of these compounds, negative giant magnetodielectric effects are shown. A positive giant magnetodielectric effect was reported in $TbMnO_3$ single crystal at low temperatures [11]. Here, the frustrated sinusoidal antiferromagnetic order induced magnetoelastic behavior was attributed for the induced polarization. In this compound, it was suggested that the spin reorientation of Mn^{3+} caused by the plausible magnetic-field-induced Tb^{3+} moment reversal changes the exchange interaction energy and then brings about the lattice modulation owing to a finite spontaneous polarization. However, no direct evidence of spin reorientation of Mn^{3+} was provided. Interestingly, magnetodielectric effects at spin reorientation originating from spin-phonon coupling are reported in Mn-substituted yttrium orthoferrite [12] and in layered perovskite magnets [13]. In the spin reorientation transition (SRT) region, the applied magnetic field is expected to induce frustration leading to the induced polarization.

Ca_2FeCoO_5 is a brownmillerite [14,15]-type compound with orthorhombic crystal structure in *Pbcm* space group with unit-cell parameters $a = 5.3626(6)$, $b = 11.0943(4)$, and $c = 14.8109(6)$ [16]. The fact that one of the short lattice parameters is doubled makes this compound rare among the brownmillerite compounds with a supercell twice the size of a regular brownmillerite unit cell. The formation of superstructure causes the formation of two sets of octahedral and tetrahedral sites. This compound also exhibits intralayer cation ordering which is rare, even among brownmillerite compounds. The tetrahedral sites exhibit complete Fe/Co ordering while the octahedral sites have certain degree of randomness [16,17]. It must be noted that the compound exhibits an overall *G*-type antiferromagnetic order with tetrahedral and octahedral sites exhibiting antiferromagnetic order individually with different ordering temperatures. Neutron-diffraction studies on this compound reveal that the spin easy axis in this compound changes from along the b axis below 100 K to along the shortest axis above 200 K through a broad spin reorientation transition [16].

Here, we report the direct evidence of strong spin-lattice coupling across the spin reorientation transition and huge magnetodielectric coupling in Ca_2FeCoO_5 compound. The compound is probed in detail by temperature-dependent magnetization, synchrotron x-ray diffraction (SXPD), Raman spectroscopy, Mossbauer spectroscopy, and complex dielectric measurements. Most importantly, the maximum value of magnetodielectricity obtained was ∼24% at the temperature value ∼220 K for the frequency of ∼5 kHz, making it worthy of industrial applications.

*Corresponding author: vasant@csr.res.in

II. EXPERIMENTAL DETAILS

The sample was synthesized by solid-state reaction method, using high-purity $CaCO_3$ (99.99%), Fe_2O_3 (99.99%), and Co_3O_4 (99.99%) as precursors. Pellets were made after a number of intermediate heating to the powder and were sintered at 1250 °C for 33 h. The synchrotron x-ray diffraction (SXRD) data were collected using a He closed cycle refrigerator (CCR) installed at BL12 Indus-II synchrotron source, Raja Ramanna Centre for Advanced Technology (RRCAT), India. The wavelength used was 0.782566 Å. The data were fitted by Rietveld refinement method [18] using FullProf software suite [19]; the fitted pattern is shown in Supplemental Material, Fig. S1 [20], and the resulting lattice parameters are $a = 5.3626(6)$, $b = 11.0940(9)$, and $c = 14.8109(4)$. The refinement results are in accordance with the previous report [16].

The Raman spectroscopy studies were carried out using a LabRam HR800 System, equipped with a 473-nm excitation source, an 1800-g/mm grating, and THMS 600 temperature-variation stage from Linkam, U.K. The magnetization measurements were carried out in zero-field cooled (ZFC), field-cooled cooling (FCC), and field-cooled warming (FCW) protocols in 20-Oe applied field using a superconducting quantum interface device vibrating sample magnetometer (SQUID-VSM) from Quantum Design Inc.

The ^{57}Fe Mossbauer measurements as a function of temperature were done in transmission mode with ^{57}Co/Rh radioactive source in constant acceleration mode with a Wissel velocity drive. Velocity calibration was done using natural Fe. Low-temperature and high-magnetic-field Mossbauer study was carried out using a Janis-make superconducting magnet with 5-T magnetic field. The dielectric measurements with parallel plate capacitor arrangement over 1 to 100 kHz were performed using an Alpha-A broadband impedance analyzer from Novo Control. Magnetic-field and temperature-dependent complex dielectric measurements from 6 to 300 K were performed using an Oxford Nanosystems Integra 9 T magnet-cryostat.

III. RESULTS AND DISCUSSION

The crystal structure of this compound is unique even in brownmillerites. The b axis is doubled due to intralayer cationic ordering. Thus, this compound supports both intra- and interlayer cation site ordering. On top of it, brownmillerites are known to show ordering of oxygen vacancies. Thus, determining the valance state of the two cations and site order is important. In order to verify the oxidation states of the two cations, i.e., Fe and Co, temperature-dependent x-ray absorption near-edge spectroscopy (XANES) was carried out at the Fe and Co K edge that is shown in Fig. 1. The overall spectra and edge position of the two cations matched with the previous report [21] confirming the 3+ valence state of the two cations. For comparison, the XANES spectrum of Fe_2O_3 standard sample is also plotted in the inset of the figure along with the zoomed view across the Fe K edge. The edge position matches exactly in the two samples, confirming the 3+ valance state of the Fe cations. It is also observed that the edge position is invariant with temperature.
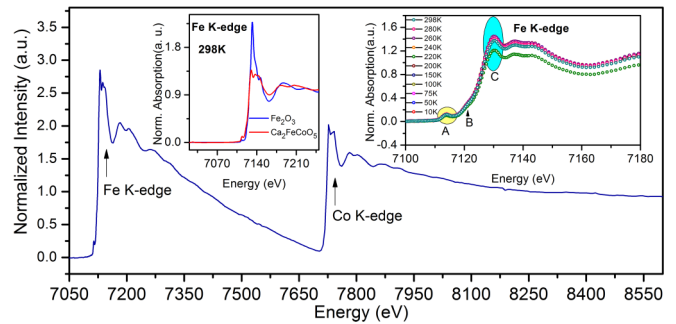

FIG. 1. XAS data of Ca_2FeCoO_5 at Fe and Co K edge. The first inset shows the Fe K-edge XANES data of Ca_2FeCoO_5 along with the reference Fe_2O_3 collected at room temperature showing that the oxidation state of Fe in the sample is +3. The second inset shows the temperatures variation of the Fe K-edge XANES indicating that the valence of the cation remains unchanged as the temperature is varied.

The magnetic structure of this compound was reported to be G-type antiferromagnetic with Néel temperature above 450 K. Most importantly, neutron-diffraction and magnetization studies showed the presence of a spin reorientation transition around 200 K. In order to verify these findings, the magnetization studies as a function of temperature were carried out and are presented in Supplemental Material, Fig. S2 [20]. The slope changes at ∼200 and ∼100 K are consistent with the reported SRT [16]. In order to investigate the magnetic structure in detail, ^{57}Fe Mossbauer spectroscopy as a function of temperature was carried out from 5 to 300 K. The Mossbauer spectra collected at different temperatures are shown in Figs. 2(a) to 2(h). As mentioned before, the Fe^{3+} ion occupies the octahedral as well as tetrahedral sites in this compound that independently exhibit antiferromagnetic order. Therefore, the spectra were fitted with two broad sextets representing octahedral and tetrahedral Fe ions. The obtained isomer shift values confirm the presence of octahedrally and tetrahedrally coordinated Fe^{3+}. The presence of sextet at 300 K is consistent with the antiferromagnetic order at room temperature, and the overall occupation of Fe at octahedral and tetrahedral sites was found to be 50.9 and 49.1%, respectively. The observation of two broad sextets with an effective field equal to about $(H_{int} \pm H_{ext})^{1/2}$ and the presence of intense $\Delta m = 0$ lines in the in-field Mossbauer data (5 K|5 T) (Supplemental Material, Fig. S3 [20]) confirms the antiferromagnetic order in the sample.

A detailed analysis of the Mossbauer spectra resulted in various values of isomer shift, quadrupole splitting, hyperfine field, etc. that are presented in Supplemental Material, Fig. S4 [20]. The temperature evolution of quadrupole splitting and the area under the sextets representing the Fe ions at octahedral (Fe_O) and tetrahedral (Fe_T) sites showed some very interesting behavior, the same is presented in Fig. 2. It must be noted that the quadrupole splitting values changed sign on lowering the temperature from 300 to 5 K for these two magnetic components at the SRT [Fig. 2(i)], which is a consequence of the change in the direction of component of electric-field gradient parallel to the internal magnetic-field direction with the spin reorientation transition [22–24]. In $Ca_2Fe_2O_5$ the ratio of Fe^{3+} distribution in tetrahedral to octahedral sites
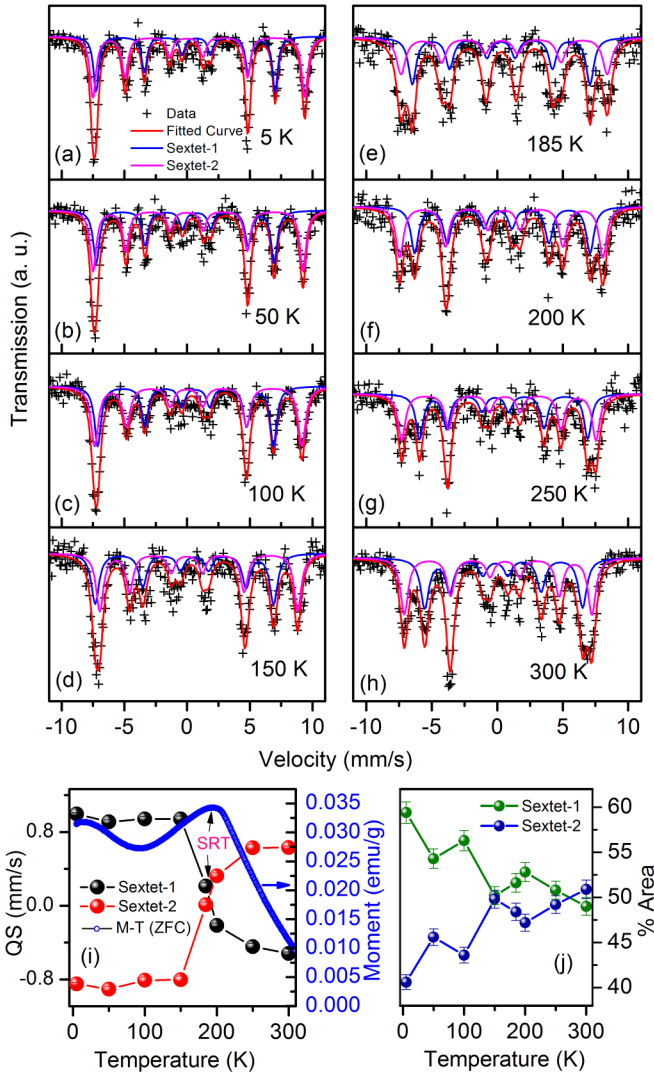
FIG. 2. Temperature-dependent Mossbauer measurements carried out from 300 to 5 K (a)–(h). Panel (i) shows the quadrupole splitting for Fe_T and Fe_O sites as a function of temperature. ZFC magnetization is also shown to mark the SRT. Panel (j) shows the % area of the overall pattern covered by different sextets representing the Fe occupation at Fe_T and Fe_O sites.

(Fe_T/Fe_O) is reported to be close to unity, determined from the relative areas of corresponding sextets considering f_O/f_T at 5 K as 0.96 ± 0.02 (f is the recoil-free fraction); however, with the doping of Ga, Sc, etc., at the Fe site the Fe_T/Fe_O ratio is found to deviate from unity [25]. In the present work, with Co doping at Fe site, the relative area ratio of Fe_T/Fe_O is found to be about 0.7 at 5 K. Interestingly, the relative area of the two sextets also showed a noticeable change with temperature [Fig. 2(j)]. Such a change is striking and can be explained by considering two possibilities: (1) the relative population of Fe cations at the octahedral and tetrahedral site is changing with temperature, or (2) the recoil-free fraction of the Fe cations at the two sites is changing with change in temperature around SRT. The first possibility is energetically very costly and hence discarded. The area of each sextuplet is directly related to the number of atoms in a particular coordination and the recoil-free fraction for the corresponding Fe nucleus.

The recoil-free fraction f is a function of the mean-square displacement of each atom [22], $f = \exp\{(-E_R)^2 \langle x^2 \rangle / \hbar c^2\}$. The most typical way to model the $\langle x^2 \rangle$ dependence is through the Debye model, which when applied to the recoil-free fraction yields

$$f = \exp\left[-\frac{3E_\gamma^2}{4Mc^2 k_B \Theta} \left(1 + \frac{4T^2}{\Theta^2} \int_0^{\Theta/T} \frac{x\,dx}{e^x - 1} \right) \right], \quad (1)$$

where E_γ is the energy of the ^{57}Fe gamma ray (14.4 keV), k_B is the Boltzmann constant, M is the mass of ^{57}Fe nucleus, c is the speed of light, and Θ is the Debye temperature for a particular nucleus. The present results can be explained only by considering drastically different Debye temperatures for the two sites. Such a variation in Θ for two sublattices is reported for spinel ferrites, garnets, etc. [26–29]. The Debye temperature is directly related with the second-order Doppler shift (SODS) [30–32]. The SODS is related with the center shift (CS) by the following relation:

$$CS(\Theta, T) = IS + SODS(\Theta, T), \quad (2)$$

where IS is the isomer shift which is nearly temperature independent while the SODS is defined as

$$SODS = -\frac{3k_B \Theta}{2Mc} \left[\frac{3}{8} + \frac{3T^4}{\Theta^4} \int_0^{\Theta/T} \frac{x^3 dx}{e^x - 1} \right]. \quad (3)$$

We have deduced the experimental values of the CS from our Mossbauer data which are presented in Supplemental Material, Table S1 [20]. Using these values and Eqs. (2) and (3), we attempted to calculate the Debye temperatures for the Fe_O and Fe_T sites. A program was constructed, in which a Debye temperature and an IS would be simulated, resulting in theoretical SODS and CS. As given in Refs. [23,32], the IS values for the Fe_O was taken as 0.61 mm/s and the variations of CS values for different Debye temperatures were simulated. Similarly, attempts were made to estimate Debye temperature for Fe_T using various values of IS and Θ. The results of this simulation are presented in Fig. 3. The Debye temperature thus estimated is found to be nearly 700 ± 50 K for the Fe_O while 225 ± 50 K for the Fe_T. These values are comparable to the values reported for $CoFe_2O_4$ [27].

The experimental points followed the theoretical trend except in the spin reorientation transition region, where it showed dramatic variation in the CS values. This variation is directly related with the variation in SODS which is a signature of lattice dynamical instability in the SRT region. Further, temperature-dependent Raman spectroscopy and SXRD studies ascertain the presence of strong spin-lattice coupling across the SRT. The evolution of Raman spectra as a function of temperature is shown in Fig. 4. Following the theoretical and experimental Raman study on brownmillerite $Ca_2Fe_2O_5$ [33], the major mode observed at $\sim$700 cm^{-1} was deconvoluted using two Lorentz functions. The Raman shifts and full width at half maximum (FWHM) thus resulting are plotted as a function of temperature and presented in Figs. 5(a) and 5(b). The Raman shift and FWHM showed anomalous behavior around the temperature window concurrent with
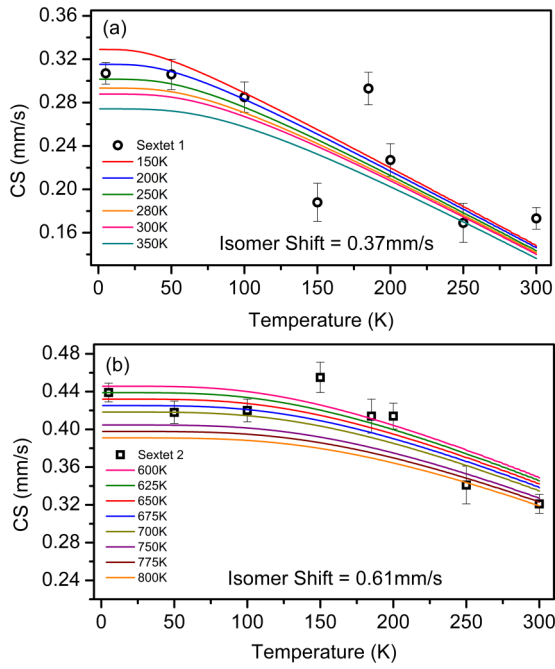
FIG. 3. Theoretically simulated lines of CSs for given Θ (solid lines) and experimental data (points) for Fe_T (a) and Fe_O (b).

the SRT. The lattice parameters deduced from SXRD are presented in Figs. 5(c)–5(f). The SXRD measurements were carried out in both heating and cooling cycle that showed a strong hysteresis. Such a hysteretic behavior was also observed in the magnetization measurements (Fig. S2) [20], confirming metastable behavior of magnetization and lattice across the SRT.

The dielectric measurements were carried out from 300 K down to 6 K, which showed strong frequency-dependent dielectric relaxation; however, the dielectric constant is rather small ($\varepsilon' < 50$), slowly varying, and nearly frequency independent below 100 K (Fig. S5) [20]. The temperature-
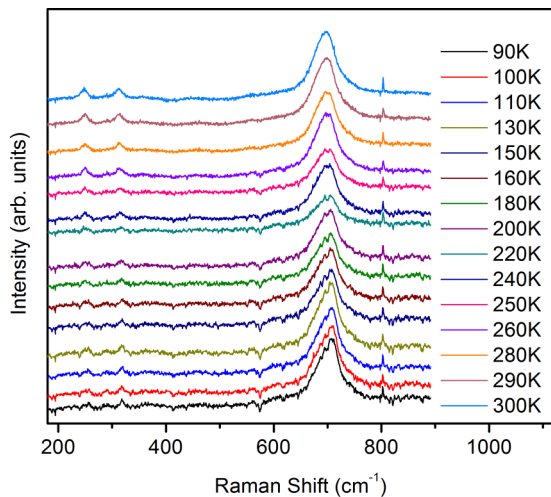

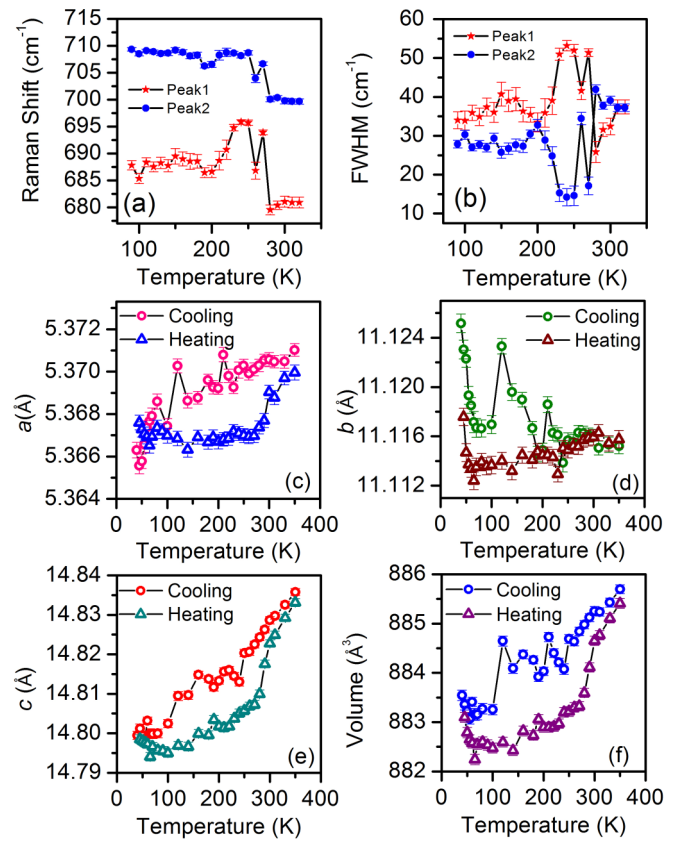FIG. 4. Temperature dependence of the Raman spectra of Ca_2FeCoO_5.

FIG. 5. (a) Raman shift and (b) FWHM of the most prominent modes as a function of temperature and the lattice parameters (c), (d), (e) as a function of temperature obtained from the refinement of SXPD data of Co_2FeCoO_5 collected in cooling and heating cycle. (f) The unit-cell volume as a function of temperature. The variations in cooling cycle parameters are higher compared to the parameters obtained in heating cycle that is attributed to poor temperature control in cooling cycle.

dependent dielectric constant showed two broad humps which are frequency dependent (dispersive).

The corresponding loss (tanδ) also showed signatures of strong dielectric relaxations (Fig. S6) [20]. Generally, Maxwell-Wagner processes are considered for explaining extrinsic effects in dielectric relaxations which arise from the grain boundaries. We attempted to measure magnetoresistance of the sample in order to detect the extrinsic contribution to the dielectric relaxations; however, the resistance was found extremely high below 250 K and was beyond our measurable limit ($>M\Omega$). Thus, the sample is highly insulating and hence, the contribution of Maxwell-Wagner-type relaxation, if at all present, is considered to be negligible. This is corroborated by the low (<100) intrinsic values of the dielectric constant and low (<1) loss tangent at low frequencies, up to 150 K. Therefore, the relaxations observed at two distinct temperatures are considered as intrinsic effect of the sample. Mossbauer spectroscopy showed that the Debye temperature corresponding to Fe ions at octahedral and tetrahedral sites are drastically different. Therefore, it is likely that the dielectric relaxations arising due to the two sites are apart in temperature. The two humps in the dielectric measurements are thus attributed to the two Debye temperatures. Figure 6(a) shows the typical
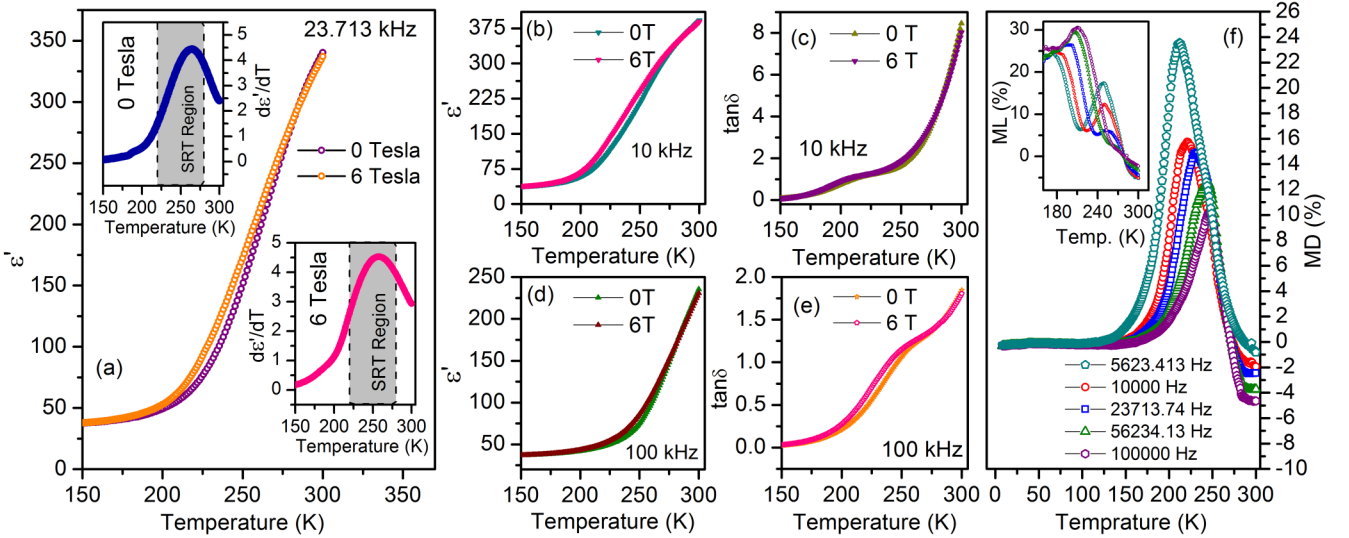
FIG. 6. (a) The dielectric constant (ε') vs temperature at 23.713 kHz measured under 0 and 6 T applied field. The upper (lower) inset shows the derivative of ε' as a function of temperature collected in 0 T (6 T) showing a peak in the SRT region. Panels (b), (d) show the dielectric constant (ε') vs temperature at typical frequencies of 10 and 100 kHz measured under 0 and 6 T, whereas panels (c), (e) show the corresponding loss tangent as a function of temperature. (f) MD (%) calculated from the ε' vs temperature data under 0 and 6 T applied field collected at different frequencies, showing a maximum value of 24% for 5623.413 Hz, whereas the inset shows the corresponding ML (%).

dielectric constant (ε') measured at $\sim$23.7 kHz in the SRT region under 0 and 6 T applied magnetic field. The insets show derivative of the ε' collected under 0 and 6 T, which shows anomaly in the SRT region. The ε' measured under 0 and 6 T applied magnetic field at 10- and 100-kHz frequencies is shown in Figs. 6(b) and 6(d). It clearly shows an enhancement in dielectric constant under field, over the temperature window across the SRT. The corresponding loss tangents are presented in Figs. 6(c) and 6(e). It also shows changes in the SRT region. This enhancement is observed at almost all the frequencies, indicating the intrinsic nature of magnetodielectric effect.

The percentage magnetodielectricity (MD) is calculated using the formula: MD(%) = [{$\varepsilon'(6\,T) - \varepsilon'(0\,T)$}/$\varepsilon'(0\,T)$] × 100 and presented in Fig. 6(f), whereas the percentage magnetoloss (ML) is calculated using the formula: ML(%) = [{$\tan\delta(6\,T) - \tan\delta(0\,T)$}/$\tan\delta(0\,T)$] × 100 for different frequencies. It is observed that the MD is unusually large in magnitude and shows a maximum value of 24% at $\sim$5 kHz which tends to decrease with increasing frequencies; however, the MD is still >10% at 100 kHz. The peak in MD shows a shift towards higher temperature with increasing frequency, reflecting the dispersion observed in ε'.

In a system with spiral magnetic order, the magnetodielectricity arises due to changes in the spiral magnetic order due to the application of external magnetic field. The external magnetic field normally destroys the spiral order, thus decreasing the induced polarization (P) and increasing the polarization susceptibility (ε'), as per observed. In TbMnO$_3$, Kimura et al. [11] argued that the Mn spin reorientation changes the exchange interaction energy and then brings about the lattice modulation owing to a finite spontaneous polarization. Following this argument, we suggest that in the SRT region the magnetic order can be considered to be "frustrated", as over

this temperature window, spins in two different directions are present as observed in our recent neutron-diffraction studies on Ca$_2$Fe$_{1.2}$Al$_{0.8}$O$_5$ [34]. In the SRT region, the landscape of the sample possesses a distribution of spatial regions corresponding to magnetic phases with different spin directions. The boundaries between the different magnetic regions are expected to show a systematic variation in spin direction leading to the development of finite spontaneous polarization (via the Dzyaloshinskii-Moriya-type spin orbit interaction). In a system which possesses strong spin-lattice coupling, the lattice modulation is allied with the SRT and thus, the induced polarization is also expected to locally modulate [35,36]. In the SRT region, the external magnetic field also alters the spin configuration, in turn changing the induced polarization. Both these effects are reflected in the changes in ε' of the sample around SRT and under the influence of magnetic field.

IV. CONCLUSIONS

In conclusion, present studies give direct evidence of correlation among spin reorientation transition and positive magnetodielectricity through strong spin-lattice coupling. The dielectric anomaly is observed across the spin reorientation transition signifying its link with the magnetism. In Ca$_2$FeCoO$_5$ compound, it is shown by Mossbauer spectroscopy that the relative area under the two sextets corresponding to octahedral and tetrahedral sites changes with temperature which has been interpreted as two distinct Debye temperatures corresponding to the octahedral and tetrahedral sites. The analysis of CS gave direct evidence of lattice instability across SRT. The strong spin-lattice coupling is reflected in modification of lattice parameters deduced from temperature-dependent SXPD and anomalous behavior of Raman modes across SRT. The magnetic-field-induced changes

in spin dynamics across the SRT bring about the lattice modulation which in turn gives rise to the giant magnetodielectric- ity. This study thus gives a route to control the magnetodielectric response due to SRT through spin-lattice coupling.

[1] M. Gajek, M. Bibes, S. Fusil, K. Bouzehouane, J. Fontcuberta, A. Barthélémy, and A. Fert, Nat. Mater. **6**, 296 (2007).

[2] M. Fiebig, T. Lottermoser, D. Meier, and M. Trassin, Nat. Rev. Mater. **1**, 16046 (2016).

[3] H. Schmid, Ferroelectrics **162**, 317 (1994).

[4] S. W. Cheong and M. Mostovoy, Nat. Mater. **6**, 13 (2007).

[5] N. A. Hill, J. Phys. Chem. B **104**, 6694 (2000).

[6] W. Eerenstein, N. D. Mathur, and J. F. Scott, Nature (London) **442**, 759 (2006).

[7] T. Kimura, Y. Sekio, H. Nakamura, T. Siegrist, and A. P. Ramirez, Nat. Mater. **7**, 291 (2008).

[8] M. A. Subramanian, T. He, J. Chen, N. S. Rogado, T. G. Calvarese, and A. W. Sleight, Adv. Mater. **18**, 1737 (2006).

[9] D. Bansal, J. L. Niedziela, R. Sinclair, V. O. Garlea, D. L. Abernathy, S. Chi, Y. Ren, H. Zhou, and O. Delaire, Nat. Commun. **9**, 15 (2018).

[10] D. Choudhury, P. Mandal, R. Mathieu, A. Hazarika, S. Rajan, A. Sundaresan, U. V. Waghmare, R. Knut, O. Karis, P. Nordblad, and D. D. Sarma, Phys. Rev. Lett. **108**, 127201 (2012).

[11] T. Kimura, T. Goto, H. Shintani, K. Ishizaka, T. Arima, and Y. Tokura, Nature (London) **426**, 55 (2003).

[12] P. Mandal, V. S. Bhadram, Y. Sundarayya, C. Narayana, A. Sundaresan, and C. N. R. Rao, Phys. Rev. Lett. **107**, 137202 (2011).

[13] B. Huang, J.-Y. Zhang, R.-K. Huang, M.-K. Chen, W. Xue, W.-X. Zhang, M.-H. Zeng, and X.-M. Chen, Chem. Sci. **9**, 7413 (2018).

[14] A. A. Colville and S. Geller, Acta Crystallogr. **B27**, 2311 (1971).

[15] R. W. Grant, S. Geller, H. Wiedersich, U. Gonser, and L. D. Fullmer, J. Appl. Phys. **39**, 1122 (1968).

[16] F. Ramezanipour, J. E. Greedan, A. P. Grosvenor, J. F. Britten, L. M. D. Cranswick, and V. O. Garlea, Chem. Mater. **22**, 6008 (2010).

[17] R. K Hona, A. Huq, and F. Ramezanipour, Inorg. Chem. **56**, 14494 (2017).

[18] H. M. Rietveld, J. Appl. Crystallogr. **2**, 65 (1969).

[19] J. Rodríguez-Carvajal, Physica B **192**, 55 (1993).

[20] See Supplemental Material at http://link.aps.org/supplemental/10.1103/PhysRevB.99.024436 for detailed characterization of Ca_2FeCoO_5 Comprising of: Rietveld refinement of room temperature SXPD data, magnetization vs temperature data, Mossbauer spectroscopy data collected at 5K with 5T magnetic field along with the parameters obtained after fitting the temperatures dependent Mossbauer data in the form of a table, temperature dependent dielectric constant along with loss tangent as a function of temperature at different frequencies for applied field of 0 Tesla showing changes in the SRT region.

[21] A. P. Grosvenor and J. E. Greedan, J. Phys. Chem. C **113**, 11366 (2009)

[22] N. N. Greenwood and T. C. Gibb, *Mossbauer Spectroscopy* (Chapman and Hall, London, 1971).

[23] M. Eibschutz, S. Shtrikman, and D. Treves. Phys. Rev. **156**, 562 (1967).

[24] I. Nowik, A. Jain, S. M. Yusuf, and J. V. Yakhmi, Phys. Rev B **77**, 054403 (2008).

[25] R. W. Grant, H. Widersich, S. Geller, U. Gonser, and G. P. Espinosa, J. Appl. Phys. **38**, 1455 (1967).

[26] J. de la Figuera, A. Quesada, L. M. García, M. Sanz, M. Oujja, M. Castillejo, A. Mascaraque, A. T. N'Diaye, M. Foerster, L. Aballe, and J. F. Marco, Croat. Chem. Acta **88**, 453 (2015).

[27] S. J. Kim, S. W. Lee, and C. S. Kim, Jpn. J. Appl. Phys. **40**, 4897 (2001).

[28] S. J. Kim, S. W. Lee, S. Y. An, and C. S. Kim, J. Magn. Magn. Mater. **210**, 215 (2000).

[29] G. A. Sawatzky, F. Van Der Woude, and A. H. Morrish, Phys. Rev. **183**, 383 (1969).

[30] V. G. Bhide and M. S. Hegde, Phys. Rev. B **5**, 3488 (1972).

[31] J. Cieslak, S. M. Dubiel, J. Zukrowski, M. Reissner, and W. Steiner, Phys. Rev. B **65**, 212301 (2002).

[32] A. Scrimshire, A. Lobera, A. M. T. Bell, A. H. Jones, I. Sterianou, S. D. Forder, and P. A. Bingham, J. Phys.: Condens. Matter **30**, 105704 (2018).

[33] A. Piovano, M. Ceretti, M. R. Johnson, G. Agostini, W. Paulus, and C. Lamberti, J. Phys.: Condens. Matter **27**, 225403 (2015).

[34] G. Sharma, V. Sathe, S. Tyagi, R. J. Choudhry, S. D. Kaushik, and V. Siruguri, Ceram. Int. **44**, 19866 (2018).

[35] N. Abe, N. D. Khanh, T. Sasaki, and T. Arima, Phys. Rev. B **89**, 054437 (2014).

[36] G. Sharma, D. Kumar, S. Tyagi, V. R. Reddy, R. Rawat, A. K. Sinha, N. P. Lalla, and V. Sathe, J. Alloys Compd. **732**, 358 (2018).